

Design of the Compact Toroid Fueler for Center Fueling Tokamak de Varennes

Roger Raman, John C. Thomas, David Q. Hwang, Garrard D. Conway, Francois Martin, Akira Hirose, Paul Gierszewski & Réal Décoste

To cite this article: Roger Raman, John C. Thomas, David Q. Hwang, Garrard D. Conway, Francois Martin, Akira Hirose, Paul Gierszewski & Réal Décoste (1993) Design of the Compact Toroid Fueler for Center Fueling Tokamak de Varennes, *Fusion Technology*, 24:3, 239-250, DOI: [10.13182/FST93-A30198](https://doi.org/10.13182/FST93-A30198)

To link to this article: <https://doi.org/10.13182/FST93-A30198>



Published online: 09 May 2017.



Submit your article to this journal 



Article views: 25



View related articles 

DESIGN OF THE COMPACT TOROID FUELER FOR CENTER FUELING TOKAMAK DE VARENNES

FUSION FUEL CYCLES

KEYWORDS: *compact toroid, spheromak, fueling*

ROGER RAMAN* *Canadian Fusion Fuels Technology Project
2700 Lakeshore Road West, Mississauga, Ontario, L5J 1K3, Canada*

JOHN C. THOMAS and DAVID Q. HWANG
*University of California-Davis, Department of Applied Science
Livermore, California 94550*

GARRARD D. CONWAY *University of Saskatchewan, Department of Physics
Saskatoon, Saskatchewan, S7N 0W0, Canada*

FRANCOIS MARTIN *Centre Canadien de Fusion Magnétique
Varennes, Québec, J3X 1S1, Canada*

AKIRA HIROSE *University of Saskatchewan, Department of Physics
Saskatoon, Saskatchewan, S7N 0W0, Canada*

PAUL GIERSZEWSKI *Canadian Fusion Fuels Technology Project
2700 Lakeshore Road West, Mississauga, Ontario, L5J 1K3, Canada*

RÉAL DÉCOSTE *Centre Canadien de Fusion Magnétique
Varennes, Québec, J3X 1S1, Canada*

Received August 18, 1992

Accepted for Publication April 28, 1993

Reactor particle fueling is one of the issues that remain to be resolved in the development of a tokamak fusion reactor. One of the most promising concepts of reactor fueling is the injection of high-speed compact toroids (CTs). Compact toroid formation and acceleration at the Ring Accelerator Experiment (RACE) device at Lawrence Livermore National Laboratory has shown that CT plasmoid velocities sufficient for center fueling fusion reactors can be achieved by using coaxial accelerators. The Compact Toroid Fueler (CTF) will inject high-speed, dense spheromak plasmoids into the Tokamak de Varennes (TdeV) to examine the feasibility of this approach as a fueler for future reactors. Here, a conceptual design study of the particle fueler for TdeV is presented. The issues of CTF

design that are considered are formation and relaxation of an axisymmetric CT, optimization of accelerator performance to improve injector electrical efficiency, separation of formation and acceleration phases to improve injector reproducibility, minimization of entrained impurities in the CT, and minimization of neutral gas load to the tokamak following CT fueling. The CTF injector will test theories on CT/tokamak interaction related to reactor fueling. Among the eventual physics questions addressed are the multiple-pulse requirements for future injectors, the bootstrap current enhancement factor, CT fuel confinement times, impurity effects, plasma heating, injector electrical efficiency, and the effect of gas load on the tokamak following CT injection.

*Current address: Centre Canadien de Fusion Magnétique, Tokamak de Varennes, 1804 Montée Ste-Julie, Varennes, Québec J3X 1S1, Canada.

I. INTRODUCTION

For long-pulse or steady-state operation of a tokamak, on-line particle fueling is needed. Continuous particle fueling by gas puffing external to the plasma is a standard technique in all tokamaks. However, this gas will not efficiently penetrate into the central core of a burning tokamak plasma, where the bulk of the fusion reaction occurs. Most of the puffed fuel will be swept away in the plasma scrape-off layer, resulting in very low burnup rates. In fact, it is necessary for the injected fuel to penetrate well beyond the tokamak magnetic separatrix. Although the optimal penetration depth is not yet clear, it is highly desirable to be able to penetrate to the plasma core to minimize tritium throughput, to improve startup ignition, and to provide full and flexible control of the plasma density profile. Two types of center-fueling schemes currently exist: (a) frozen pellet injection and (b) neutral beam injection. For central penetration of an International Thermonuclear Experimental Reactor (ITER) class reactor, frozen pellet velocities of up to 100 km/s may be needed.¹ Conventional pneumatic injectors have attained velocities of up to 3 km/s (Ref. 2), while 10 km/s appears possible with advanced systems. This is still an order of magnitude less than desired. The low inertial strength of frozen pellets further exacerbates the problem by limiting the acceleration pressure and consequently requiring impractically long (length \gg tokamak dimensions) acceleration sections for reactor center fueling. The neutral beams are optimally designed for plasma heating, and while successfully used for fueling on a small scale, e.g., Joint European Torus (JET) tritium shots, they are too inefficient for fueling purposes. Inefficiency refers to the amount of fuel injected per unit of energy consumed by the fueler.

Recent work by Perkins et al.,¹ Parks,³ and Newcomb⁴ indicates that central fueling of reactor-grade tokamak plasmas may be possible by compact toroid (CT) injection, specifically by spheromak injection. However, it is important to note that the work of Newcomb, Perkins et al., and Parks are all theoretical treatments. The spheromak is a CT plasma configuration with approximately equal strengths of toroidal and poloidal magnetic fields. Beginning in the early 1980s, major experiments on the spheromak concept were conducted at Los Alamos National Laboratory (LANL) with the Compact Toroid Experiment (CTX) device,⁵ Princeton University with the S1 device,⁶ University of Maryland with the MS device,⁷ and Osaka University with the CTCC-I device.⁸ At LANL, the CTX device⁹ has demonstrated the formation of relatively clean spheromaks as indicated by the electron temperature of ~ 100 eV, which exceeds the oxygen radiation barrier temperature. The corresponding flux confinement time was several hundred microseconds. At the Lawrence Livermore National Laboratory (LLNL) Ring Accelerator Experiment¹⁰⁻¹² (RACE), spheromak trans-

lational velocities of up to 2500 km/s have been demonstrated for low-mass CTs ($\ll 10 \mu\text{g}$), while velocities of ~ 1400 km/s have been achieved with CTs weighing $\sim 20 \mu\text{g}$. The net acceleration efficiency defined as CT kinetic energy divided by the initial capacitor bank energy was $\geq 30\%$. Compact toroid formation efficiencies are generally $\geq 10\%$ for an unoptimized system.¹³ The overall system efficiency (unoptimized, formation plus acceleration) is $\geq 20\%$. The rather high efficiencies achieved in this scheme combined with the plasma parameters achieved to date, which exceeds the more modest requirements thought necessary for tokamak fueling,¹ make this a strong contender for tokamak reactor fueling.

Initial experiments by Brown and Bellan^{14,15} demonstrated that it is possible to increase the density and current of a toroidal plasma by CT injection. However, in their experiment, the particle content of the target tokamak (ENCORE, major radius = 38 cm) was small in relation to the injected CT ($N_{\text{CT}} \sim 6 \times N_{\text{tokamak}}$, where N is the total particle inventory). This resulted in the tokamak discharge being quenched soon after CT injection. The injection of accelerated CTs into a tokamak plasma and the effects of accelerated CT impurities on the target tokamak (for a nonquenched tokamak discharge) have not been studied.

For CT fueling to be proven viable, accelerated CT injection into a medium-sized, well-diagnosed tokamak ($N_{\text{CT}} \leq 0.3 \times N_{\text{tokamak}}$) with acceptable impurity levels needs to be demonstrated. The goal of the Compact Toroid Fueler (CTF) is to perform such a proof-of-principle experiment at the Tokamak de Varennes (TdeV) facility (major radius = 86 cm). Initial commissioning and testing of the injector will be done at the University of Saskatchewan.

The main physics goals to be investigated are the following:

1. maximum fuel mass that can be injected without causing a tokamak disruption. This information will be used in future injectors to determine the multiple-pulse requirements.
2. tokamak plasma density profile perturbation and possible control via CT injection
3. CT impurities and levels, methods to limit their level, and effect of CT impurities on the tokamak
4. injection of CTs with hydrogen, deuterium, and helium plasmas to simulate CT tritium injection
5. particle confinement time of the CT fuel during centrally fueled discharges. This allows an estimate of the fuel burnup fraction that can be expected during CT tritium fueling of future reactors
6. extent of additional plasma heating due to the substantial kinetic energy of the CT

7. extent of enhancement in bootstrap current due to CT fueling. Since the bootstrap current is proportional to the radial pressure gradient, this effect is expected to be much higher than during pellet fueling.

The technology goals are as follows:

1. to measure CT injection electrical efficiency
2. to measure and minimize CT impurities
3. to measure and minimize residual gas loads on the tokamak.

This paper is divided into three parts. Section II describes the design considerations and technical implementation of the CT injector. Section III deals with the problem of impurity control crucial to tokamak fueling devices. Section IV briefly discusses the relevant CT tokamak diagnostics pertinent to CT injection.

II. CT FORMATION AND ACCELERATION

II.A. Injector Requirements

Table I lists the representative TdeV parameters, and Table II is a list of the desired CT parameters. For a proof-of-principle experiment, a 5 to 30% perturbation of the TdeV particle inventory is desired. The necessary inventory of particles should be contained in a CT small enough to pass through a port on TdeV and small compared with the minor diameter of the tokamak. This limits the CT diameter to <15 cm. Given these parameters for the CT mass and size, the Perkins et al. model predicts central fueling for CT velocities of ~40 to 60 cm/μs; the primary requirement is that the CT kinetic energy exceed the displaced toroidal magnetic field energy of the tokamak. In general, the temperature of these CT plasmas will be limited to ~10 eV, as energy loss from these plasmas will be dominated by line radiation from trace carbon and oxygen impurities. Even if compressed to high densities, on time scales relevant to this experiment (a few

TABLE I
TdeV Machine and Plasma Parameters

Major radius, R (cm)	86
Minor radius, a (cm)	27
Plasma volume (cm ³)	1.27×10^6
Average density, $\langle n_e \rangle$ (cm ⁻³)	1.85 to 7.4×10^{13}
Peak density, $n_{e \text{ peak}}$ (cm ⁻³)	2.7 to 8.3×10^{13}
Particle inventory, N_{tot}	$2.3 \text{ to } 9.4 \times 10^{19}$
Toroidal field on axis, B (T)	1.5
Electron temperature, T_e (eV)	700
Z_{eff}	1.4 to 1.5
Plasma thermal energy, E (kJ)	5
Helicity (Wb ²)	-0.15

microseconds), the temperature is not expected to rise above 20 eV since <1% oxygen is needed to clamp the temperature at about the oxygen radiation barrier temperature (for $n_e > 10^{15} \text{ cm}^{-3}$). However, because of the high translational velocities, the energy per ion is substantial (e.g., 2.5 keV/ion). Since this energy will ultimately be converted to thermal energy after interaction with the tokamak plasma, this fueling scheme has the additional benefit of serving as a plasma-heating mechanism. This is an advantage over pellet fueling, which cools the tokamak plasma after fuel deposition. With proper control of the fuel deposition profile, the substantial kinetic energy of the CT plasma may lead to an enhanced bootstrap current. A comparison of the helicity content of the CT and the tokamak shows that the current drive due to helicity injection will be negligible in this experiment because of the small volume of the CT (volume of tokamak ~ 500 × volume of CT) despite the 1-T CT fields after compression. For the current drive from helicity injection to be significant, the CT volume (for similar tokamak CT magnetic fields) should be of comparable magnitude to the tokamak volume. This, however, would result in the CT particle inventory also being of comparable magnitude to the tokamak particle inventory, a regime not desirable for particle fueling purposes. Finally, the magnetic binding energy per ion, which is related to the plasma beta, is high in the spheromak (unpublished RACE results). This means that the spheromak is a robust structure, a feature desirable for the CT/tokamak interaction process.

II.B. The CTF Injector

The CTF injector is very similar in concept to the RACE device,¹² and in general, the design has many

TABLE II
Desired CT Parameters

Particle inventory, N_{CT} (particle)	$2.3 \text{ to } 28 \times 10^{18}$
Plasma density, n_{CT} (cm ⁻³)	$8.3 \times 10^{14} \text{ to } 1 \times 10^{16}$
Fueling of TdeV inventory (%)	5 to 30
Mass, m_{CT} (μg)	4 to 47
Outer radius, r_{out} (cm)	7
Inner radius, r_{in} (cm)	3.5
Length, L_{CT} (cm)	20
Volume, $V_{\text{ol,CT}}$ (cm ³)	<2500
Average magnetic field, $\langle B_{\text{CT}} \rangle$ (T)	1
Magnetic energy, W_{CT} (kJ)	1
Translational velocity, $V_{\text{el,CT}}$ (cm/μs)	10 to 100
Plasma beta, β (%)	<5
Electron temperature, $T_{e,\text{CT}}$ (eV)	<20
Plasma thermal energy (J)	22 to 270
Plasma kinetic energy (J)	19 to 12 000
Equivalent energy per ion (eV)	25 to 2609
Helicity (Wb ²)	$\sim 10^{-5}$
Magnetic binding energy per ion (keV)	0.5 to 6

similarities to the RACE device. The impressive results achieved on the RACE device played an inspirational role in the design of CTF. Figure 1 schematically shows the main features of the CTF injector. As in RACE, the CTF injector consists of four regions: the formation, precompression, acceleration, and focusing regions.

II.B.1. The Formation Region

This region consists of two coaxial stainless steel formation electrodes and oxygen-free high-conductivity

(OFHC) copper entrance region electrodes. The stainless steel electrodes are 71 cm long with diameters of 16.8 cm (outer) for the inner electrode and 24.8 cm (inner) for the outer electrode. To the rear of the injector is a 22-cm-diam, 10-cm-long alumina cylinder that provides an electrical break between the electrodes. On either side of the break are stainless steel flanges that are connected to an 800- μ F, 10-kV capacitor bank via 16 coaxial cables (RG 218); the inner electrode is the cathode, and the outer electrode (the anode) is the ground. Figure 2 shows the associated electrical schematic. Inside the inner formation electrode is a solenoid

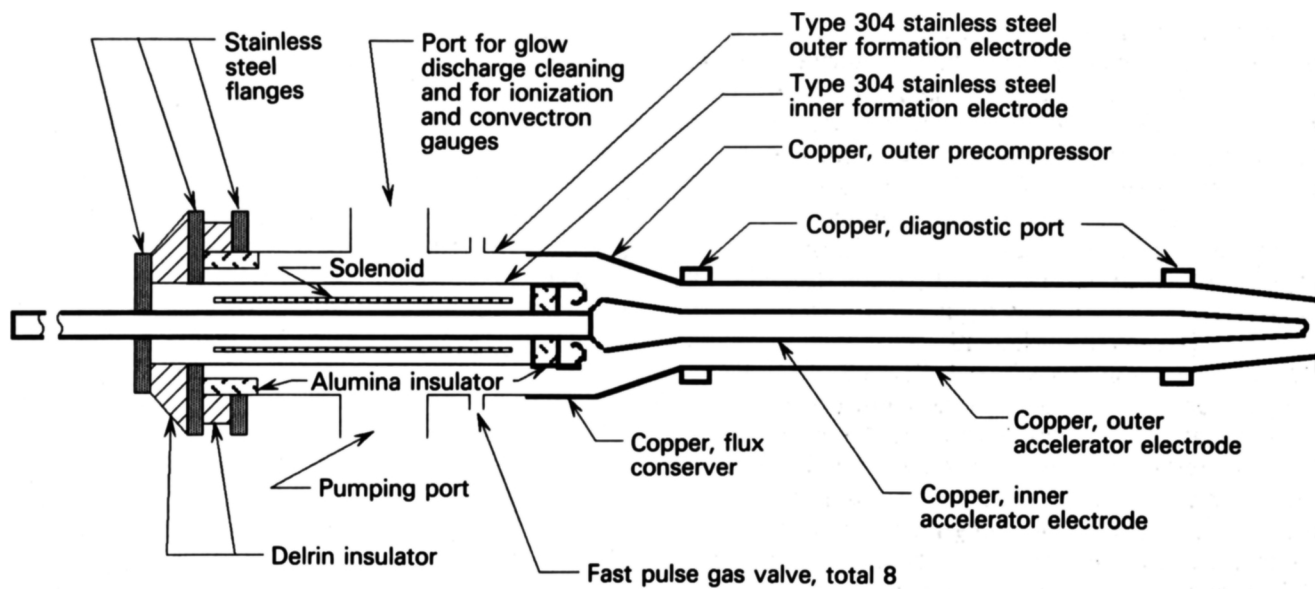


Fig. 1. Schematic of the CTF machine.

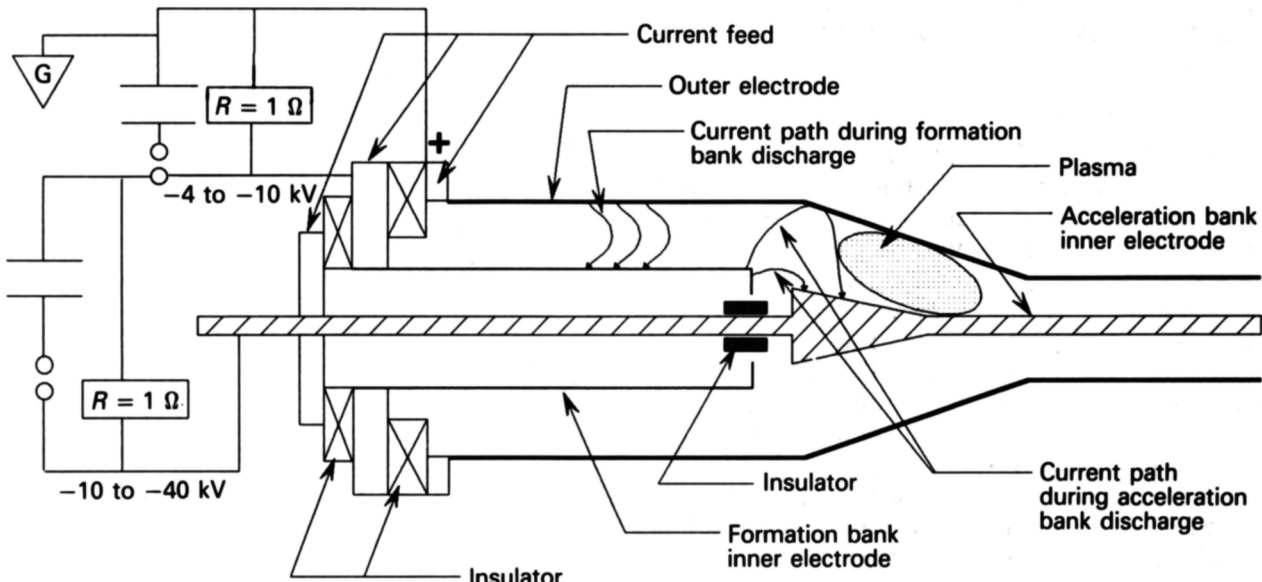


Fig. 2. CTF electrical schematic.

powered by a 3-kV, 1500- μ F capacitor bank capable of generating up to 6 mWb of magnetic flux. Type 304 stainless steel was chosen for the formation electrodes since they needed to be resistive enough to allow the solenoidal flux to penetrate through them. The outer electrode forms the vacuum chamber and has two 20-cm (8-in.)-diam ports. The bottom port is connected to a 1000 l/s (Edward's magnetically levitated) turbomolecular pump, while the top port contains ionization and convection gauges, as well as provisions for *in situ* residual gas analysis during glow discharge cleaning. To the right of the pump port are eight pulsed gas injection valves equally spaced azimuthally. The valves are powered in parallel by two ($C = 200 \mu$ F and $V = 2$ kV) capacitor modules. The valves (designed by the University of California-Davis CTIX group and later modified by the University of Saskatchewan group) are fast acting and provide up to 10^{19} particles per pulse per valve. Eight valves were necessary to provide a uniform gas distribution in the annulus between the electrodes in as short a time as possible. Approximately 15 cm is required axially on either side of the gas valve port to trap an adequate amount of particles in the CT (for high-mass CTs). With a neutral hydrogen transit time of ~ 0.1 cm/ μ s, $\sim 150 \mu$ s is required to completely fill the discharge chamber. Alternatively, to form low-mass CTs, the formation gun will be discharged at the instant the gas front reaches the inner electrode ($\sim 16 \mu$ s after the gas exits the nozzle). Further to the right of the stainless steel electrodes is the 14-cm-long OFHC copper entrance nozzle. In general, the nozzle should be flux conserving and have a length equal to a few times the interelectrode gap distance. These attributes serve three purposes. First, they isolate the forming CT from the resistive stainless steel electrodes. Second, they provide a flux-conserving region in which the solenoidal flux can stretch and easily detach at the nozzle exit because of a sharp jump in the inner electrode radius. Third, they isolate the solenoid flux from the acceleration flux.

II.B.2. CT Formation

Figure 3 outlines the steps involved in CT formation and acceleration. The solenoid is energized first ($t = 0$). The solenoidal flux penetrates the stainless steel electrodes and creates a footprint on both electrodes. Footprints are the regions where the flux enters and leaves a surface. The gas valves are pulsed near the time of peak solenoid flux ($t \sim 2$ ms). The neutral hydrogen gas fills the annulus between the electrodes; then, after a suitable delay, the formation capacitor bank is discharged to ionize the gas. The current density \mathbf{J} between the electrodes coupled with the toroidal field \mathbf{B}_{tor} it generates results in a force $\mathbf{J} \times \mathbf{B}$ that accelerates the plasma toward the entrance region. The solenoidal flux (poloidal flux) will offer resistance to the flowing plasma because of field line tension. If the gun current I_g exceeds a critical value I_{crit} , then the gun $\mathbf{J} \times \mathbf{B}$ force

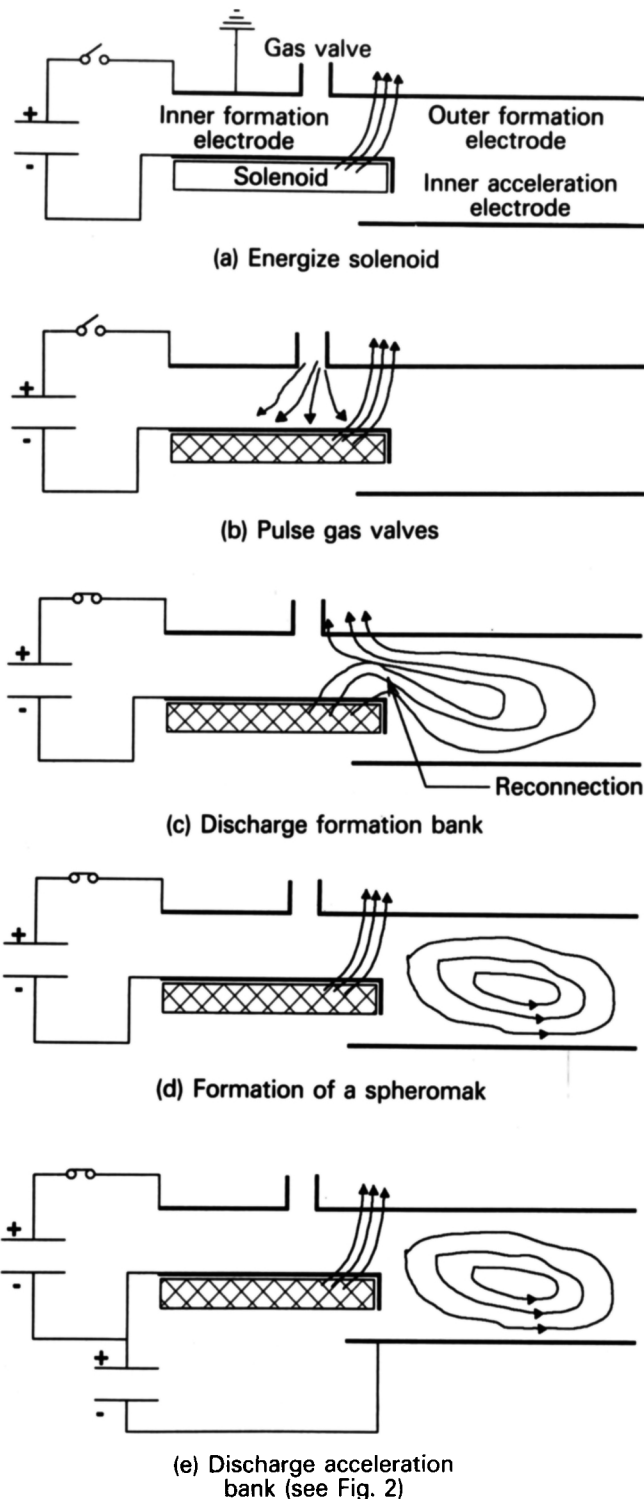


Fig. 3. CT formation and acceleration.

exceeds the restraining tension and a CT is formed. This is described by the following relation¹⁶:

$$\text{CT formation if } \lambda_g \equiv \frac{\mu_0 I_g}{\phi_g} > \frac{\mu_0 I_{crit}}{\phi_g}, \quad (1)$$

where

- λ_g = helicity eigenvalue (or energy per unit helicity)
 ϕ_g = solenoidal flux.

Physically, this states that for the condition $I_g > I_{crit}$, it is energetically favorable for CT formation to occur, or from a geometric perspective, the volume containing the solenoidal flux becomes smaller than that available in the entrance region. Current theories¹⁷ predict that long cylindrical entrance regions should have a characteristic energy per unit helicity given by

$$\lambda_{threshold} = \frac{C}{r_e} , \quad (2)$$

where

- r_e = radius of the flux conserver or entrance region
 C = constant dependent on the model used.

In our case, the plasmoid that will form in the flux conserver would be oblate because of the shape of the flux conserver. Finn et al.¹⁸ and Bondeson et al.¹⁹ solved the eigenvalue equation $\nabla \times \mathbf{B} = \lambda \mathbf{B}$ for a spheromak in a flux conserver, where λ is again the helicity eigenvalue that satisfies the boundary condition for the flux conserver of interest. For $L/R < 1.67$ (L and R are the length and radius of the flux conserver), the minimum energy state is axisymmetric. If $L/R > 1.67$, the spheromak is nonaxisymmetric. For our case, $L/R < 1.67$, so that an oblate axisymmetric spheromak should result. The current-to-flux ratio for this case is given by the following relation:

$$\lambda_g \equiv \frac{\mu_0 I_g}{\phi_g} = \frac{3.83}{r_e} , \quad (3)$$

where the constant $C = 3.83$ is the first root of the Bessel function $J_1(x)$. This relation, however, is not in agreement with experiments. Barnes et al.²⁰ state that there may be an uncertainty factor of 2 in the constant between theory and experiment. Brown et al.²¹ point out that the relation

$$\lambda_g = \frac{\pi}{\delta_{gap}} \quad (4)$$

shows better agreement with their experiments. Here, δ_{gap} is the difference in radii between the inner and outer electrodes. For our case, Eq. (4) results in $\lambda_g = 80 \text{ m}^{-1}$, while Eq. (3) results in $\lambda_{gun} = 30 \text{ m}^{-1}$. For 3 mWb of solenoid flux, $\lambda_{gun} = 80 \text{ m}^{-1}$ results in a threshold gun current of $\sim 200 \text{ kA}$, while $\lambda_{gun} = 30 \text{ m}^{-1}$ results in $\sim 75 \text{ kA}$. However, both yield critical current values less than the design value of 360 kA for the formation bank.

The CT that forms in the flux conserver will decay as the internal currents are dissipated because of plasma resistivity. The magnetic diffusion equation for a resistively decaying spheromak is given as¹³

$$\frac{\partial \mathbf{B}}{\partial t} = \frac{-\eta \lambda^2 \mathbf{B}}{\mu_0} , \quad (5)$$

where η is the Spitzer resistivity. The decay time τ thus is given by

$$\tau_{mag} = \frac{\mu_0}{\eta \lambda^2} . \quad (6)$$

If $T_e \sim 10 \text{ eV}$, then $\eta = 4 \times 10^{-5} \Omega \cdot \text{m}$, and for $\lambda = 30 \text{ m}^{-1}$ (which is the value in the flux conserver), then $\tau_{mag} \sim 30 \mu\text{s}$. In general, in CTX and other experiments, an anomaly factor of 3 has been noted between the prediction of Eq. (6) and the experimental value. The predicted magnetic decay time in our experiment may therefore be $\sim 10 \mu\text{s}$. This would then result in a plasma lifetime of $\sim 30 \mu\text{s}$ (about three times the e -folding time). Brown et al. point out that in their experiment an anomaly of 5 to 10 is seen between the predicted and measured e -folding times of the magnetic fields in the California Institute of Technology (Caltech) spheromak discharge.²² This large anomaly may be because the Caltech spheromak was injected into the ENCORE tokamak vessel, while other spheromaks were injected into cylindrical flux conservers.

Once formed, the CT may or may not be nonaxisymmetric. However, since the spheromak equilibrium in an oblate flux conserver requires it to be axisymmetric, an initially nonaxisymmetric CT will become axisymmetric after a relaxation period. This relaxation time is on the order of a magnetic reconnection time and is given by the following relation¹⁶:

$$\tau_{relax} = S^f \tau_{Alfvén} , \quad (7)$$

where

S = magnetic Reynolds number (anticipated to be ~ 600 in CTF)

f = fraction of the order of $\frac{1}{2}$ to $\frac{1}{3}$.

This means that ~ 3 to $7 \mu\text{s}$ is needed for the CT to relax in the flux conserver. To decouple the CT formation phase from the acceleration phase, it is important that the plasma lifetime exceed the sum of the helicity injection time plus the CT relaxation time. The formation bank's first quarter cycle time in the present injector configuration is $\sim 14 \mu\text{s}$, so that by proper adjustment of the solenoid flux, the helicity injection phase may be limited to as low as $5 \mu\text{s}$. Thus, it is anticipated that the acceleration phase can be initiated ~ 10 to $15 \mu\text{s}$ after the helicity injection into the source chamber begins.

II.B.3. CT Acceleration

Compact toroid acceleration occurs in the pre-compression, acceleration, and focusing regions of the device. The precompressor is the region that separates the formation section from the accelerator and serves two important purposes. First, it allows the formation of a relatively large spheromak that can then be reduced to the required final size. Since the flux confinement time of these plasmoids scales as r^2 , it is advantageous to form as large an initial spheromak as possible. As the spheromak is compressed to its final dimensions, its lifetime will correspondingly decrease. However, since the acceleration phase lasts for $<10\ \mu\text{s}$, the compressed CT will exit the accelerator before excessive flux loss occurs. Furthermore, during the precompression phase, which may last as long as $5\ \mu\text{s}$, magnetic energy density in the spheromak will increase because of compression. Second, the precompressor allows the separation of the formation and acceleration processes and allows time for the source plasmoid to relax and stabilize before acceleration, thus ensuring that the relaxed and hence accelerated CT will more likely be axisymmetric. Also, since in this gun geometry the acceleration phase is independent of formation, the accelerator bank timing becomes less critical (as compared with dynamic formation and acceleration). This should result in more reproducible CTs.

In this injector, the precompressor reduces the inner and outer radii of the source spheromak from 5 and 12 cm to ~ 3.5 and 7 cm, respectively, in the accelerator. This compression is obtained by discharging the accelerator bank across the inner formation electrode (biased positive) and the inner acceleration electrode (biased negative) as shown in Fig. 2. The resulting $\mathbf{J} \times \mathbf{B}$ force compresses the CT against the cone of the precompressor, while eddy currents in the cone wall provide a restraining force. With increasing current in the circuit, the CT is compressed until it becomes small enough to enter the accelerator region. Once in the straight accelerator, there is no axial restraining force, and the CT accelerates very rapidly. The transit time along the 1-m-long accelerator section is expected to be $\leq 4\ \mu\text{s}$ (much less for low-mass CTs).

In this injector, a final focusing section has been added. Its purpose is to allow proper interfacing with the tokamak. Here, part of the CT kinetic energy is used to further compress the CT, allowing it to pass unobstructed through the 15-cm (6-in.)-diam gate valve and port that separate the injector from the tokamak.

The precompressor, accelerator, and focusing geometries were optimized by using the TRAC code developed at LLNL (Refs. 11 and 12). The TRAC code is a two-dimensional ideal magnetohydrodynamic (MHD) Lagrangian code that tracks the group motion of the CT through the different phases of precompression, acceleration, and focusing. The code has shown good agreement with the results of the RACE experiment.^{11,12}

The code allows for arbitrary variation of the accelerator/precompressor geometry as well as the external circuit parameters. Based on simulations, a $100\text{-}\mu\text{F}$, 40-kV capacitor bank with an external inductance of $\sim 150\ \text{nH}$ was chosen for the CT injector accelerator bank. Figure 4 shows an example of the ultimate performance that is expected from this injector.

Figure 4 shows contours of the Lagrangian grid, poloidal field, toroidal field, velocity, and density at 3, 4, 6, and $7\ \mu\text{s}$ into the simulation. The Lagrangian grid plot shows the location of the CT in the injector. The remaining plots, which are enlarged to show the grid, provide details of magnetic field, velocity, and density. Time zero corresponds to the accelerator bank firing time. The large jump in the Lagrangian grid (at $t = 7\ \mu\text{s}$) occurs because the code attempts to establish a suitable boundary with the few particles that have high velocity. Examination of the toroidal field contour shows that the bulk of the CT is well localized to inner and outer radii of 2.6 and 6.25 cm and a length of 20 cm. Future versions of the TRAC code (under development by J. Eddleman) will incorporate an Eulerian grid that will avoid such numerical ambiguities. It should be noted that this is not a real problem. The simulation is for a 40-kV bank charge voltage and 10-mW external resistance. Here, a 40- μg -mass CT with an initial average field of $\sim 1\ \text{T}$, in the formation chamber, is compressed to a final field of $\sim 2.5\ \text{T}$ and a final velocity of $\sim 70\ \text{cm}/\mu\text{s}$ (at the exit of the acceleration section). The peak current in the circuit is $\sim 380\ \text{kA}$, which is much less than the acceleration power system capability of $\sim 550\ \text{kA}$. At $3\ \mu\text{s}$, the plasmoid has moved out of the horizontal flux-conserving region and is prevented from moving further by the restraining pressure offered by the cone section. The peak poloidal field is $\sim 1.3\ \text{T}$, and the bulk fluid velocity of the CT is $<5\ \text{cm}/\mu\text{s}$. The circuit current is 300 kA. At $t = 4\ \mu\text{s}$, the circuit current exceeds 350 kA, and there is sufficient force available to compress the CT into the accelerator region. In the accelerator, the peak poloidal field increases to $2.5\ \text{T}$, and the bulk fluid velocity increases to $\sim 25\ \text{cm}/\mu\text{s}$. During the next $3\ \mu\text{s}$, the CT traverses the 1-m-long accelerator section and is further compressed in the focusing section. In this simulation, the CT that leaves the focusing region enters a drift tube region. In actual fueling experiments, the drift tube would, of course, be replaced by the tokamak. The toroidal field contour at $7\ \mu\text{s}$ shows that the CT has an outer radius of $\sim 6.25\ \text{cm}$ at $z = 190\ \text{cm}$, which is less than the 7.0-cm inner radius of the drift tube. Since the focusing section ends at $z = 147\ \text{cm}$, this represents a flight over a distance of 43 cm without contacting the drift tube walls. In reality, the length of the CTF/Tdev interconnecting region is only 12.3 cm, so that the CT should enter the tokamak without contacting any CTF/Tdev interfacing components. The final bulk fluid velocity is $\sim 70\ \text{cm}/\mu\text{s}$, the peak poloidal field is $1.6\ \text{T}$, and the peak density is $5 \times 10^{-8}\ \text{g}/\text{cm}^3$ or

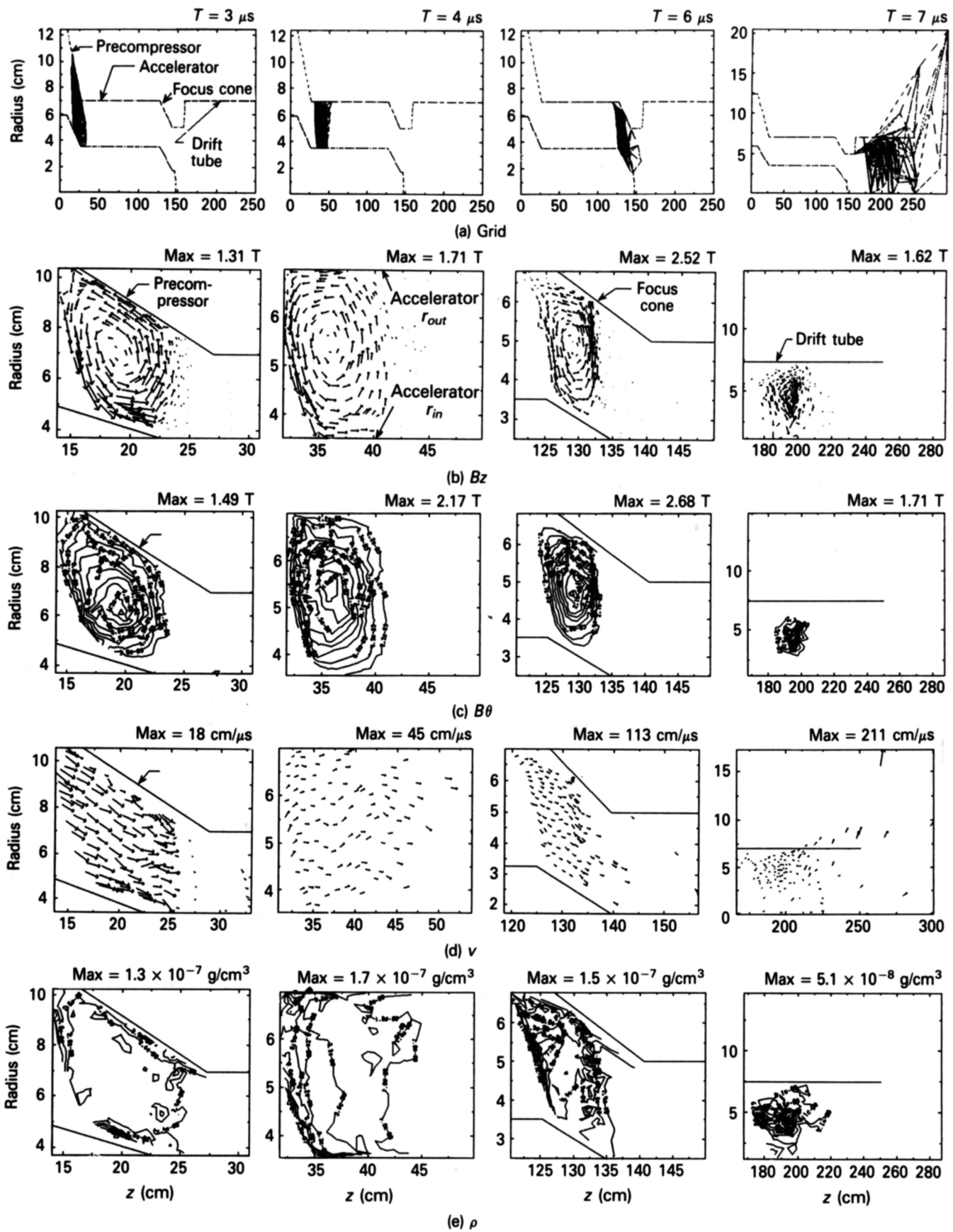


Fig. 4. Contours of Lagrangian grid, poloidal field, toroidal field, velocity, and density (top to bottom) at 3, 4, 6, and 7 μ s (left to right) after initiation of CT acceleration. The radial and z axes are not the same scale.

$3 \times 10^{16} \text{ cm}^{-3}$. Figure 5 shows that the final magnetic energy is $\sim 900 \text{ J}$, while the CT has attained a final kinetic energy of 12 kJ .

III. IMPURITY CONTROL

An essential requirement for any fueling device is that the injected fuel should entrain minimal levels of impurity. After considerable effort, CTX at LANL managed to generate CTs with low levels of impurity as indicated by the relatively high electron temperature and long plasma lifetime.^{9,23} This was achieved only after plasma spray coating the electrodes with tungsten and extensive glow discharge cleaning.

When using spheromaks for fueling, it is preferable for the CT to be radiation dominated at a known and acceptable impurity fraction. For a radiation-dominated plasma, the electron temperature is low, therefore allowing the number of fuel particles in the CT to be maximized through the finite beta limitation. This condition can easily be met with $< 1\%$ oxygen needed to clamp the temperature at the radiation barrier level for a density $\geq 10^{15} \text{ cm}^{-3}$. An estimate of the maximum allowable level of impurities introduced into the TdEV (if oxygen) may be obtained, for a proof-

of-principle experiment, by limiting the CT Z_{eff} to between 2 and 3. Assuming that the oxygen is fully stripped (conservative), up to 2% oxygen may be contained in the CT to give a Z_{eff} of 2, and 5% for a Z_{eff} of 3. Thus, for this experiment, between 2 to 5% oxygen would be an acceptable level of contamination.

In the Caltech experiment, of the six electrode coatings tested (steel, copper, nickel, chromium, rhodium, and tungsten), helicity injection into the ENCORE tokamak was noticed for only the tungsten and chromium electrodes. Apparently, in the case of the other electrodes, the helicity decay time was just short enough so that the spheromak helicity decayed below their threshold of measurement.^{22,24} Spectroscopic observations inside the tokamak (in the wavelength range of 527 to 572 nm) showed the appearance of only about ten additional lines upon spheromak injection. They attribute this to inefficient transport of high-Z impurities from the ablated electrodes. In their CTCC-I spheromak, Uyama et al.⁸ also note that high-Z impurities are not transported together with hydrogen because of inefficiency of acceleration due to their large mass, and high-Z impurities are left behind in the entrance region or in the interelectrode region as fast magnetic reconnection occurs during spheromak formation. In CTCC-I, the degree of impurity contamination in the spheromak

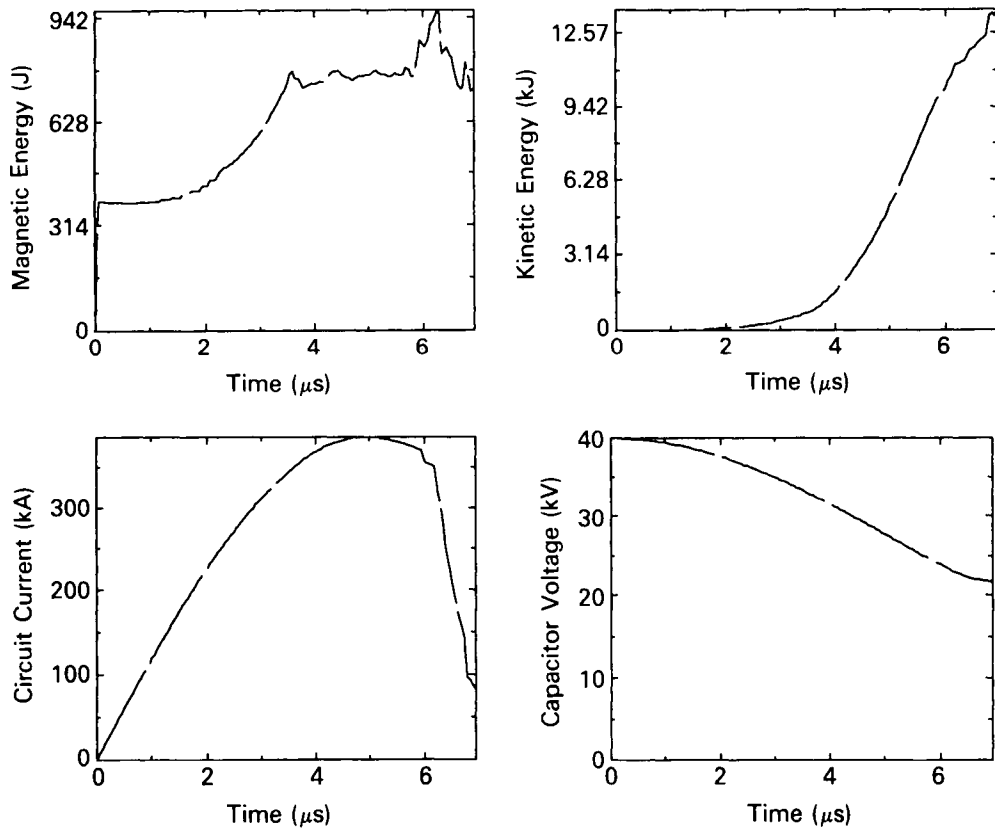


Fig. 5. CT magnetic energy, kinetic energy, external circuit current, and capacitor bank voltage as a function of time. The simulation shows peak magnetic and kinetic energies of ~ 0.9 and 12 kJ , respectively.

plasma mainly depended on the surface conditions of the flux-conserving wall. After the flux-conserver surface was coated with titanium, a large decrease in the line radiation from carbon and oxygen was observed. More recently, RACE experimental results also indicate the dominant impurity lines to be those of oxygen. The high- Z elements are either absent or negligible compared with oxygen lines. These observations are consistent with those in the CTCC-I device.⁸ The indication that CTs preferentially collect only low- Z particles may turn out to be an unexpected and desirable feature of this type of CT fueler.

Impurities in the CTF injector will mainly be controlled by the plasma spray coating of the electrode surfaces with low-porosity (high-density, ~95% theoretical density) tungsten, followed by extensive glow discharge cleaning. While the tungsten-coated electrodes in RACE result in relatively clean plasmas (as far as high- Z elements are concerned), the RACE electrodes are somewhat porous. Hartman²⁵ estimated the theoretical density of the tungsten coating on the RACE electrodes to be ~85%. A porous coating will store gas that fuels the discharge, making it more difficult to form low-mass CTs (Ref. 22). Therefore, a high-density, nonporous coating should, besides producing clean CTs, allow the injector to operate in the low-mass regime, thereby extending the parameter range available for experiments. It is noted that the Caltech experiment observed the appearance of iron and carbon lines and the CTX experiment observed the appearance of nitrogen lines. Iron is less likely to be observed in CTF as all stainless steel components exposed to primary electrical discharge are coated with dense tungsten. The appearance of carbon may be related to the specifics of the insulator material and to the details of injector design. Since the CTF design has many similarities to the RACE device, impurity behavior in CTF should be closer to the RACE experimental observations than to other spheromak guns.

Finally, while oxygen and nitrogen appear to be the dominant impurities in a single-shot injector, they are expected to be less of a problem for multishot fuelers. At a pressure of $\sim 10^{-6}$ Torr, the time it takes to form an impurity monolayer on the electrode surfaces is of the order of a few seconds; therefore, for an injector operating at a few hertz, there should be insufficient time for impurity monolayers to form between discharges, leading to a progressive self-cleaning of the electrodes. However, further research is needed to investigate and quantify the specific effects of multiple-pulsed CT gun operation.

IV. DISCUSSION

The injection of a CT plasma into a tokamak plasma can be divided into two phases. The first is the penetration phase. After leaving the gun, the CT is ex-

pected to expand and tilt while crossing the tokamak magnetic field lines.¹ This is expected to be followed by a reconnection to the tokamak magnetic field lines and diffusion of the CT plasma. It is noted that the results of Brown et al. are in conflict with the Perkins et al. model.^{14,15} This may be related to the relatively large size of the Caltech spheromak in relation to the ENCORE tokamak, which made the injection nonlocal. The ratio r_{tok}/r_{sph} was ~ 1.6 for the Caltech experiment, while it is >4 for the CTF experiment. Here, r_{tok} refers to the tokamak minor radius, and r_{sph} refers to the nominal spheromak radius. The results of the Caltech experiment as well as the validity of the Perkins et al. model needs to be investigated further by other experiments.

In CTF, the injection velocity will be adjusted so that reconnection and fueling take place at the desired location in the tokamak plasma. In the reconnection process, part of the CT kinetic energy is expected to be converted to thermal energy, thereby heating the plasma. This will happen if the kinetic energy of the CT fuel particles exceeds the thermal energy of the tokamak ions and electrons. Otherwise, the injected CT will cool the tokamak plasma, as observed in the Caltech experiment.¹⁴ The second phase is the relaxation of the perturbed tokamak plasma following fueling from the CT.

Therefore, in the context of CT injection, the diagnostics required to measure the plasma parameters can be divided into two broad categories according to their time scale: microsecond and millisecond time scale. The dynamics of the CT plasma formation and injection are on the microsecond time scale, whereas the bulk tokamak plasma parameters evolve on the slower particle confinement (millisecond) time scale. The majority of the tokamak diagnostics operate on the slower time scale and must be modified if it is desired to follow the evolution of the injected CT plasma and its interaction with the tokamak plasma. Table III lists the main TdEV diagnostics pertinent to CT injection studies.²⁶⁻²⁸

The CT specific diagnostics provide information on the mass and velocity of the CT that is injected. Helium-neon interferometer measurements will allow an estimate of the CT mass, whereas the magnetic probes will provide information on the CT magnetic content and its velocity.

As for the tokamak diagnostics, the submillimetre (SMM) interferometer will provide density distribution measurements to characterize the evolution of the deposition profile following CT injection. The effect of trace impurities in the CT plasma on the tokamak plasma will be monitored by soft X rays and visible spectroscopy. An estimate of the particle confinement time can be obtained by injecting deuterium into a hydrogen plasma. SMM interferometry and charge-exchange measurements of the injected species will provide information on its lifetime in the tokamak plasma.

TABLE III
TdeV Diagnostics Pertinent to CT Injection

Diagnostic	Parameter	Comments
Fast-framing camera	CT image	10 frame/ μ s
X-ray tomography	MHD (T_e, Z, n_e)	Five filtered arrays, full two-dimensional at 100 kHz
SMM interferometer	$n_e(r, t)$	Seven channels at 393.6 μ m, 10-kHz profile sampling
SMM polarimetry	$J(r, t)$	Six channels at 393.6 μ m
Thomson scattering	$T_e(r, t_n)$	Multiple pulse (50 Hz), four spatial channels
Mirnov coils	\tilde{B}_ϕ	14 poloidal + 4 toroidal coils, ≤ 250 kHz
CO ₂ scattering	\tilde{n}_e	$6 < k < 180$ cm ⁻¹ , $\omega < 3$ MHz
Z_{eff} meter	$Z_{eff}(r, t)$	Eight channels, visible bremsstrahlung
VUV-I spectroscopy	$T_i(r, t)$	Doppler broadening
VUV-II spectroscopy	n_{I-low}	Multispectral line
Magnetic flux coils	$R_p(t), I_p(t)$	0.5-ms resolution

Plasma heating resulting from CT injection can be measured with Thomson scattering for the electrons and by charge-exchange and high-resolution spectroscopy on the impurity lines for the ions. Finally, a fast-framing camera will monitor the propagation of the CT within the tokamak.

V. CONCLUSIONS

The CTF injector is designed to increase the TdeV particle inventory by ~ 5 to 30%. This will be achieved with the injection of a CT spheromak plasmoid traveling at a velocity of up to 1000 km/s and trapped magnetic field of ~ 1 T in a CT volume of 1 to 3 ℓ with a mass between 4 to 47 μ g. The large magnetic binding energy of the spheromak should assist in maintaining its structure upon impact with the tokamak plasma. Plasma spray coating the electrode surfaces with dense tungsten, followed by extensive glow discharge cleaning should allow the generation of relatively clean CTs of both low and high mass. With future multiple-pulse operation, this type of injector is expected to generate even cleaner CTs.

The physics studies at TdeV are expected to answer many questions in regard to CT fueling. Among these are the multiple-pulse requirements of future injectors, the bootstrap current enhancement, CT fuel confinement times, impurity effects, and plasma heating.

ACKNOWLEDGMENTS

The technical assistance provided by the CTIX and RACE groups and the University of Saskatchewan Physics Workshop is gratefully acknowledged. In particular, we would like to thank H. McLean, J. L. Eddleman, D. Ranscroft, C. Hartman, A. Molvik, and J. Hammer. Special thanks to J. Ratzlaff, H. Meredith, and T. Jarboe for the useful technical discussions. We would like to thank the reviewers for their useful comments.

REFERENCES

1. L. J. PERKINS, S. K. HO, and J. H. HAMMER, "Deep Penetration Fuelling of Reactor-Grade Tokamak Plasmas with Accelerated Compact Toroids," *Nucl. Fusion*, **28**, 8, 1365 (1988).
2. L. MARTINIS, F. SCARAMUZZI, A. FRATTOLILLO, S. MIGLIORI, A. REGGIORI, G. RIVA, and G. B. DAMINELLI, "A New Two-Stage Pellet Injector for FTU," *Proc. 13th Int. Symp. Fusion Engineering*, Knoxville, Tennessee, October 2-6, 1989, p. 1248, Institute of Electrical and Electronics Engineers (1989).
3. P. B. PARKS, "Refuelling Tokamaks by Injection of Compact Toroids," *Phys. Rev. Lett.*, **61**, 12, 1364 (1988).
4. W. A. NEWCOMB, "Magnetohydrodynamic Wave Drag," *Phys. Fluids B*, **3**, 1818 (1991).
5. J. C. FERNANDEZ et al., "Energy Confinement Studies in Spheromaks with Mesh Flux Conservers," *Nucl. Fusion*, **28**, 9, 1555 (1988).
6. M. YAMADA, "S-I Spheromak," *Nucl. Fusion*, **25**, 9, 1327 (1985).
7. R. S. SHAW and J. M. FINN, "Axisymmetric Equilibria in the Maryland Spheromak," *Nucl. Fusion*, **27**, 1309 (1987).
8. T. UYAMA et al., "Temporal Evolution of the Decaying Spheromak in the CTCC-I Experiment," *Nucl. Fusion*, **27**, 799 (1987).
9. T. R. JARBOE, F. J. WYSOCKI, and J. C. FERNANDEZ, "Progress with Energy Confinement Time in the CTX Spheromak," *Phys. Fluids B*, **2**, 1342 (1990).
10. J. H. HAMMER et al., "Experimental Demonstration of Acceleration and Focusing of Magnetically Confined Plasma Rings," *Phys. Rev. Lett.*, **61**, 25, 2843 (1988).

11. A. W. MOLVIK et al., "Quasistatic Compression of a Compact Torus," *Phys. Rev. Lett.*, **66**, 2, 165 (1991).
12. J. H. HAMMER et al., "Experimental Demonstration of Compact Torus Compression and Acceleration," *Phys. Fluids B*, **3**, 2236 (1991).
13. W. C. TURNER et al., "Investigations of the Magnetic Structure and the Decay of a Plasma-Gun-Generated Compact Torus," *Phys. Fluids*, **26**, 1965 (1983).
14. M. R. BROWN and P. M. BELLAN, "Spheromak Injection into a Tokamak," *Phys. Fluids B*, **2**, 1306 (1990).
15. M. R. BROWN and P. M. BELLAN, "Current Drive by Spheromak Injection into a Tokamak," *Phys. Rev. Lett.*, **64**, 18, 2144 (1990).
16. C. W. BARNES, J. C. FERNANDEZ, and I. HENINS, "Experimental Determination of the Conservation of Magnetic Helicity from the Balance Between Source and Spheromak," *Phys. Fluids*, **29**, 10, 3415 (1986).
17. M. J. SCHAFER, "Exponential Taylor States in Circular Cylinders," *Phys. Fluids*, **30**, 160 (1987).
18. J. M. FINN, W. M. MANHEIMER, and E. OTT, "Spheromak Tilting Instability in Cylindrical Geometry," *Phys. Fluids*, **24**, 1336 (1981).
19. A. BONDESON et al., "Tilting Instability of a Cylindrical Spheromak," *Phys. Fluids*, **24**, 1682 (1981).
20. C. W. BARNES et al., "The Impedance and Energy Efficiency of a Coaxial Magnetized Plasma Source Used for Spheromak Formation and Sustainment," *Phys. Fluids B*, **2**, 1871 (1990).
21. M. R. BROWN, D. M. CUTRER, and P. M. BELLAN, "Motion and Equilibrium of a Spheromak in a Toroidal Flux Conserver," *Phys. Fluids B*, **3**, 5, 1198 (1991).
22. M. R. BROWN et al., "Characterization of a Spheromak Gun: The Effect of Refractory Electrode Coatings," *J. Appl. Phys.*, **69**, 9, 6302 (1991).
23. T. R. JARBOE et al., "The Ohmic Heating of a Spheromak to 100 eV," *Phys. Fluids*, **27**, 13 (1984).
24. M. R. BROWN and P. M. BELLAN, "Efficiency and Scaling of Current Drive and Refuelling by Spheromak Injection into a Tokamak," *Nucl. Fusion*, **32**, 7, 1125 (1992).
25. C. HARTMAN, Lawrence Livermore National Laboratory, Personal Communication (Aug. 1991).
26. J. L. LACHAMBRE, "The Multichannel Submillimeter Wave Interferometer of TdEV," *Far Infrared Sci. Technol.*, **66**, 179 (1986).
27. H. H. MAI, J. M. LARSEN, and K. DIMOFF, "A High Speed Programmable Detector System for Plasma Spectroscopy," *Rev. Sci. Instrum.*, **57**, 866 (1986).
28. J. CASTRACANE, Y. DEMERS, and H. H. MAI, "EUV Impurity Measurements on the TEXTOR Tokamak," *Plasma Phys. Controlled Fusion*, **29**, 759 (1987).